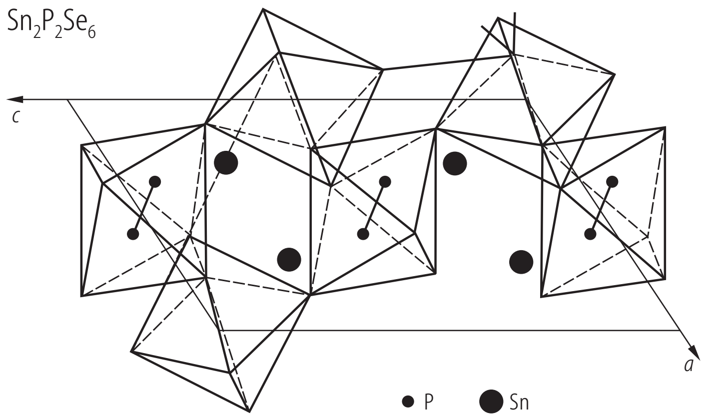

Fig. 24A-2-001. $Sn_2P_2Se_6$. Structure of phase I [88Vor]. Projection on (010) plane. Two kinds of octahedra represent P_2Se_6 and Se_6, respectively.

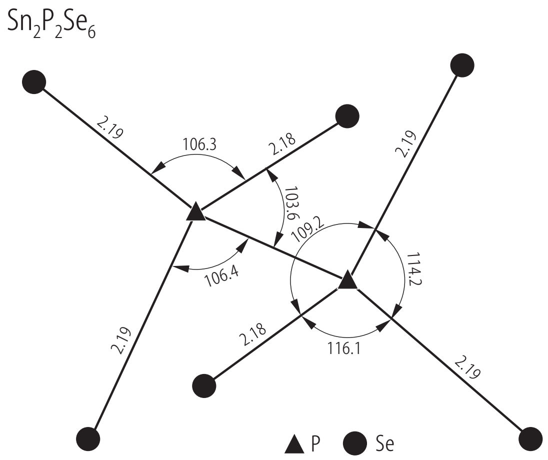

Fig. 24A-2-002. $Sn_2P_2Se_6$. Structure of phase I [88Vor]. Fragment of the structure of P_2Se_6 with interatomic distances [$Å^2$] and bond angles [°].

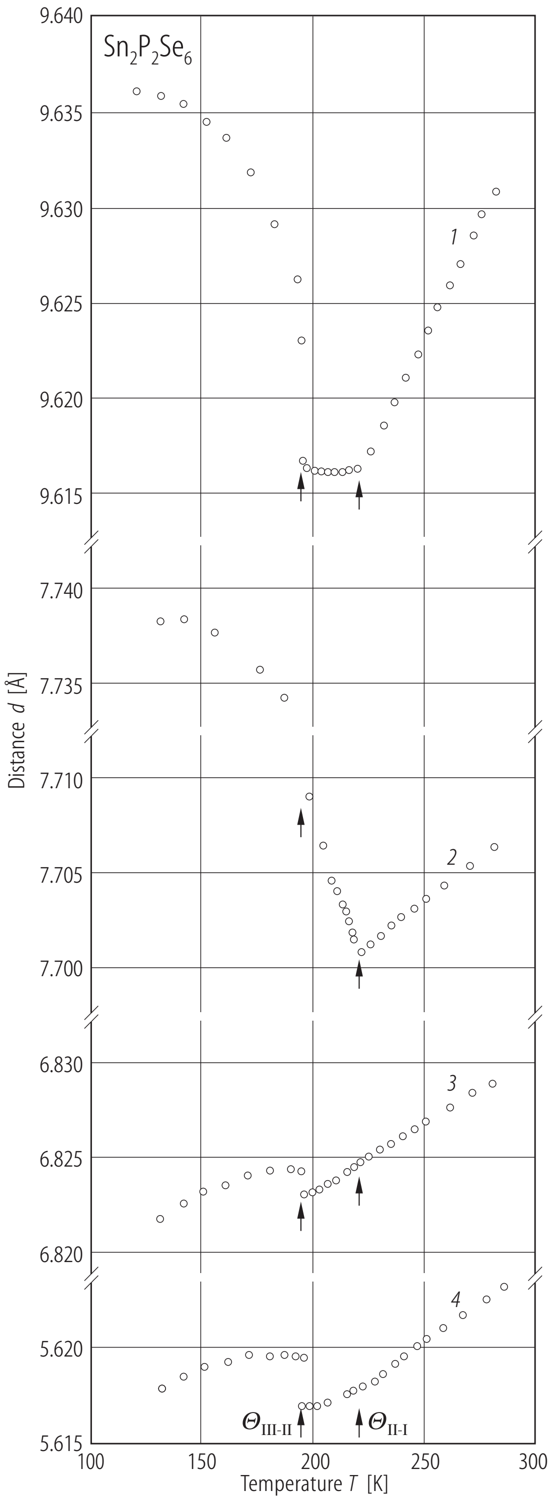

Fig. 24A-2-003. $Sn_2P_2Se_6$. *d* vs. *T* [89Par]. *d*: interplanar distance. 1: *d* (001), 2: *d*(010), 3: *d* ($\bar{1}$01), 4: *d*(100).

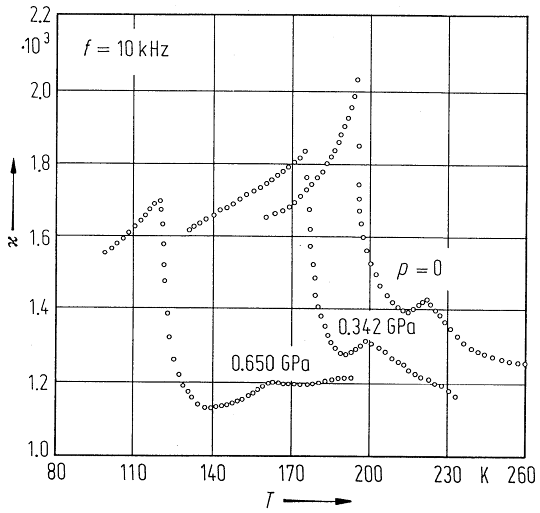

Fig. 24A-2-004. $Sn_2P_2Se_6$. κ vs. T [85Vys]. Parameter: p.

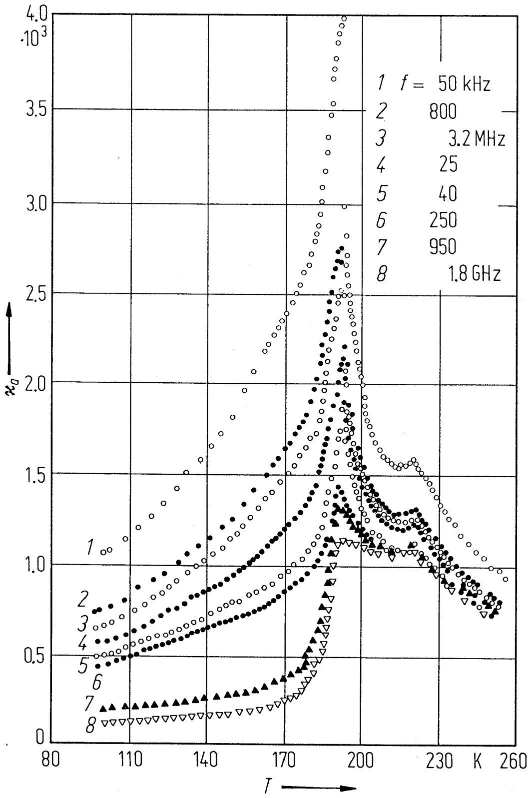

Fig. 24A-2-005. $Sn_2P_2Se_6$. κ_a vs. T [85Mai]. Parameter: f.

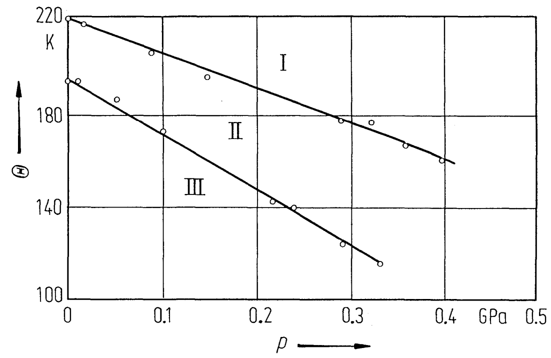

Fig. 24A-2-006. $Sn_2P_2Se_6$. Θ vs. p [85Sli].

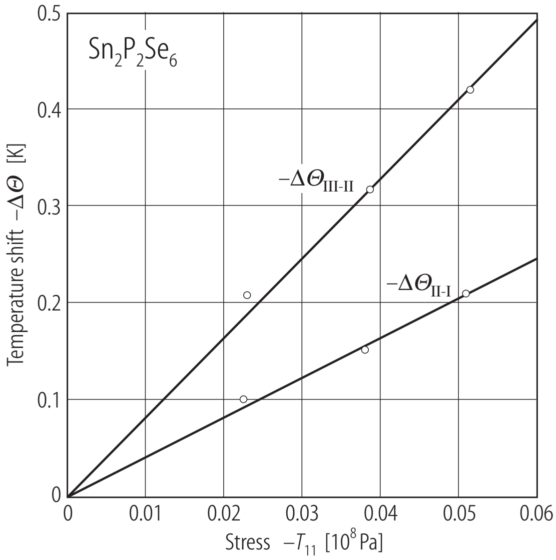

Fig. 24A-2-007. $Sn_2P_2Se_6$. $-\Delta\Theta_{II-I}$, $-\Delta\Theta_{III-II}$ vs. $-T_{11}$ [94Riz]. $\Delta\Theta_{II-I}$, $\Delta\Theta_{III-II}$: shift of Θ_{II-I} and Θ_{III-II}, respectively. Based on the axial system of the space group $P2_1/n$.

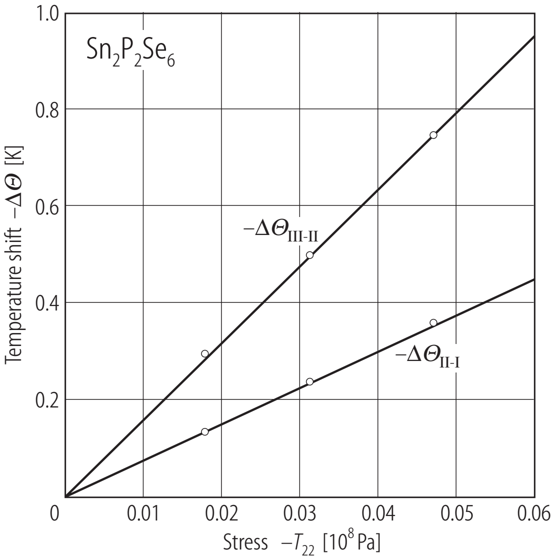

Fig. 24A-2-008. $Sn_2P_2Se_6$. $-\Delta\Theta_{II–I}$, $-\Delta\Theta_{III–II}$ vs. $-T_{22}$ [94Riz]. $\Delta\Theta_{II–I}$, $\Delta\Theta_{III–II}$: shift of $\Theta_{II–I}$ and $\Theta_{III–II}$, respectively. Based on the axial system of the space group $P2_1/n$.

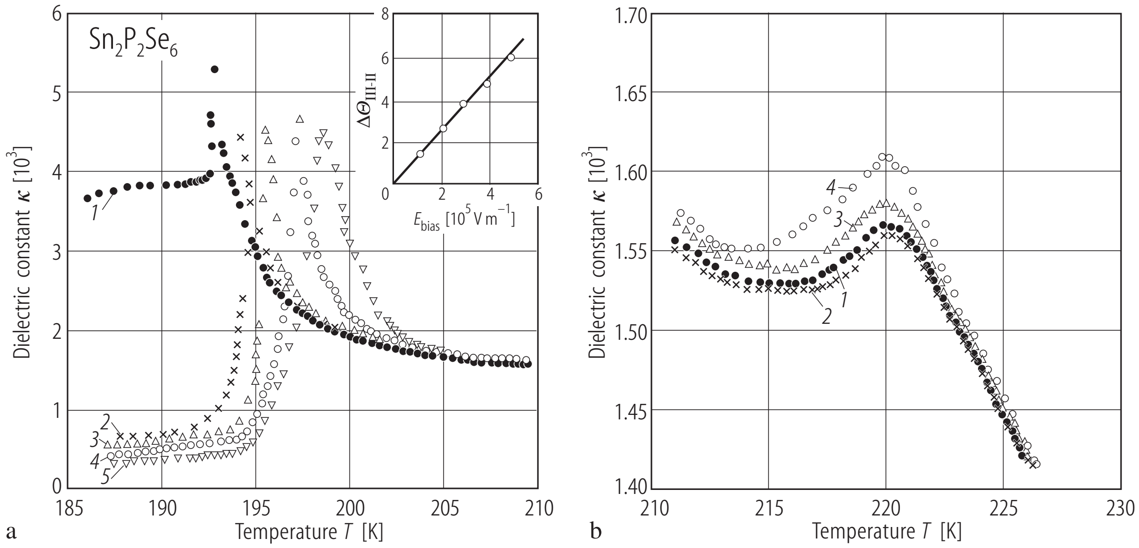

Fig. 24A-2-009. $Sn_2P_2Se_6$. κ vs. T [92Mai]. Parameter: E_{bias}. *1*: E_{bias} = 0 V m^{-1}, *2*: 1 · 10^5 V m^{-1}, *3*: 2 · 10^5 V m^{-1}, *4*: 4 · 10^5 V m^{-1}, *5*: 5 · 10^5 V m^{-1}. Insert: $-\Delta\Theta_{III–II}$ vs. E_{bias}. $\Delta\Theta_{III–II}$: shift of $\Theta_{III–II}$.

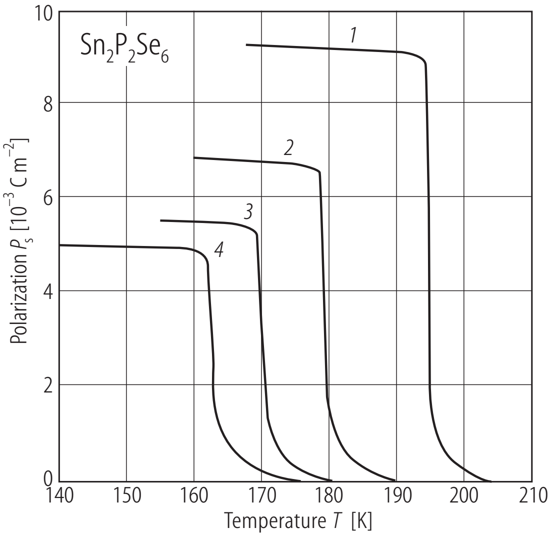

Fig. 24A-2-010. $Sn_2P_2Se_6$. P_s vs. T [92Gur]. Parameter: p. *1*: 0.0001 GPa, *2*: 0.060 GPa, *3*: 0.110 GPa, *4*: 0.140 GPa. Obtained from pyroelectric current measurements.

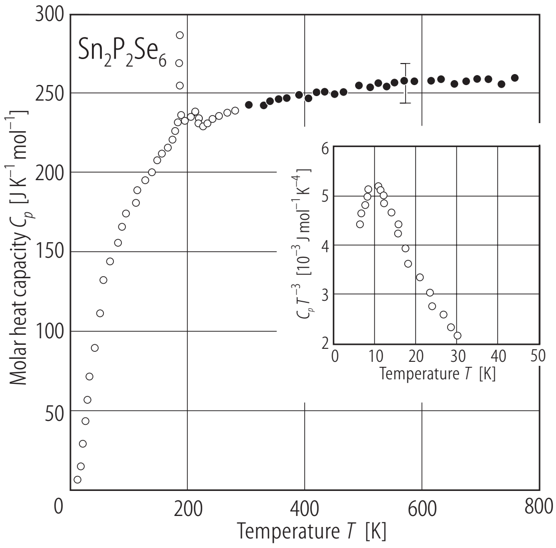

Fig. 24A-2-011. $Sn_2P_2Se_6$. C_p vs. T [94Vas]. Insert: C_p/T^3 vs. T. C_p: molar heat capacity at constant pressure.

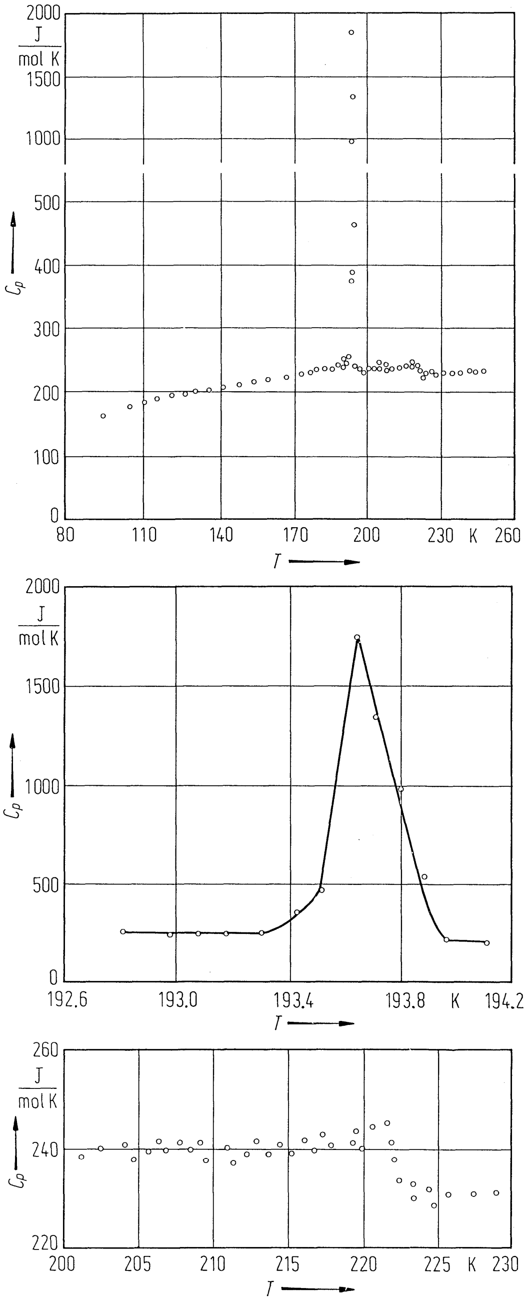

Fig. 24A-2-012. $Sn_2P_2Se_6$. C_p vs. T [83Mai]. C_p: molar heat capacity at constant pressure.

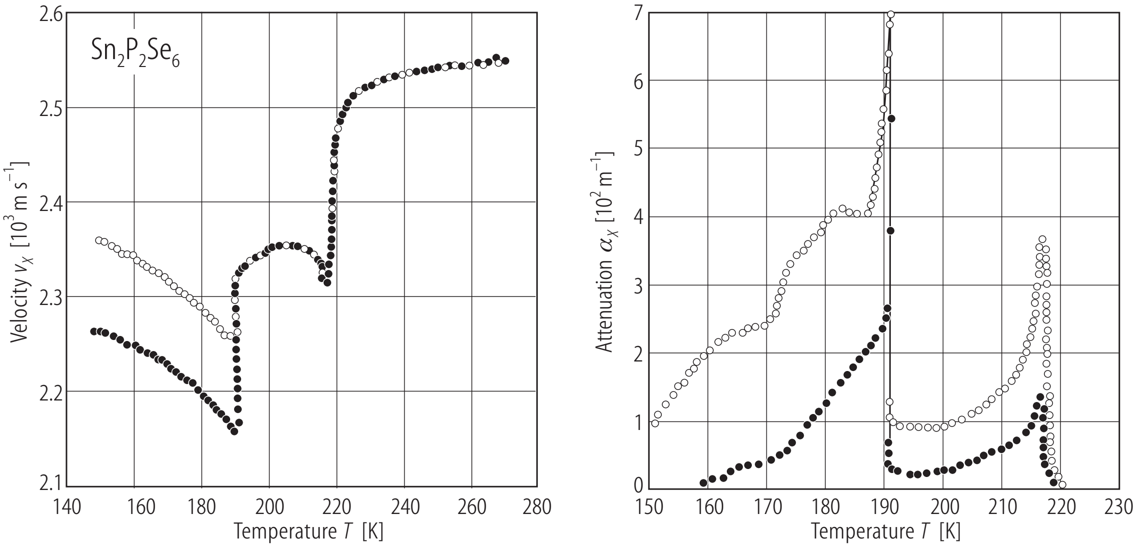

Fig. 24A-2-013. $Sn_2P_2Se_6$. υ_X, α_X vs. T [89Val]. Parameter: f. υ_X, α_X: velocity and attenuation coefficient of the longitudinal sound propagating along the X (|| [101]) direction. Full circle: f = 10 MHz, open circle: f = 30 MHz. Cooling.

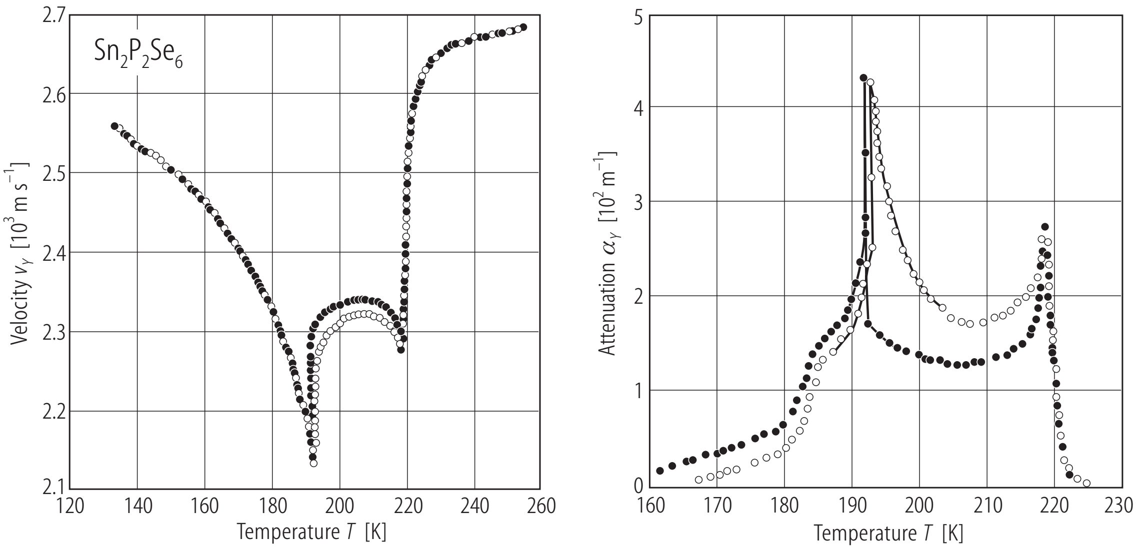

Fig. 24A-2-014. $Sn_2P_2Se_6$. υ_Y, α_Y vs. T [89Val]. υ_Y, α_Y: velocity and attenuation coefficient of the longitudinal sound propagating along the Y (|| [010]) direction. f = 10 MHz. Full circle: cooling, open circle: heating.

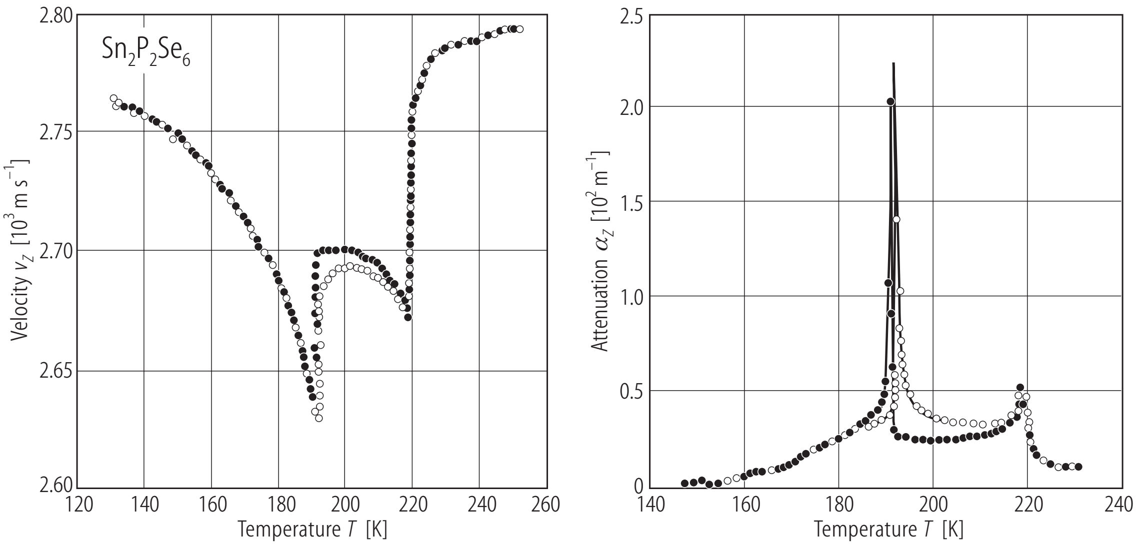

Fig. 24A-2-015. $Sn_2P_2Se_6$. υ_Z, α_Z vs. T [89Val]. υ_Z, α_Z: velocity and attenuation coefficient of the longitudinal sound propagating along the Z (||[001]) direction. f = 10 MHz. Full circle: cooling, open circle: heating.

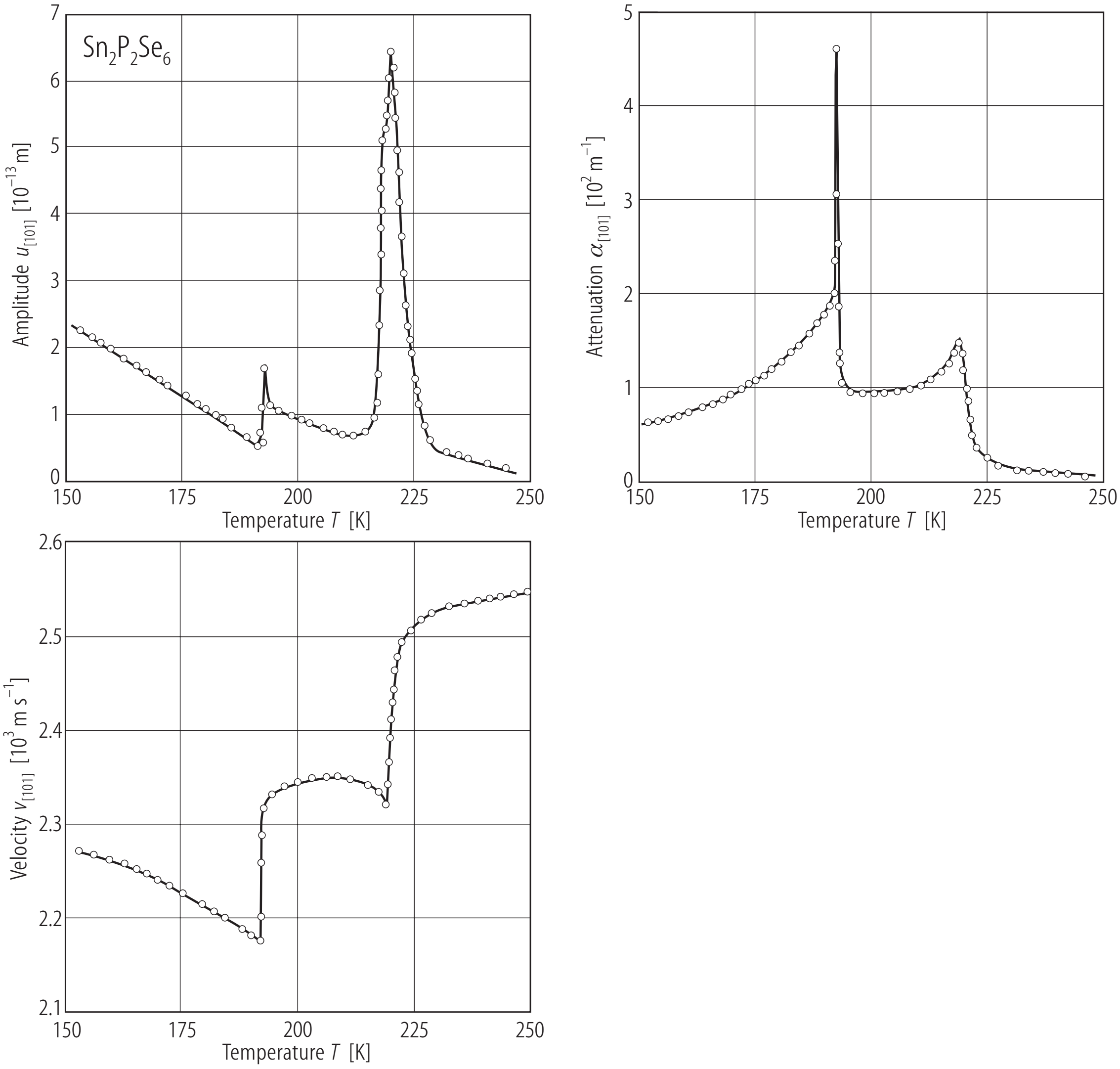

Fig. 24A-2-016. $Sn_2P_2Se_6$. $\upsilon_{[101]}$, $\alpha_{[101]}$, $u_{[101]}$ vs. T [90Sam]. $\upsilon_{[101]}$, $\alpha_{[101]}$: velocity and attenuation of the longitudinal ultrasound (10 MHz) propagating along the polar [101] direction, $u_{[101]}$: amplitude of the second longitudinal ultrasonic harmonic (20 MHz).

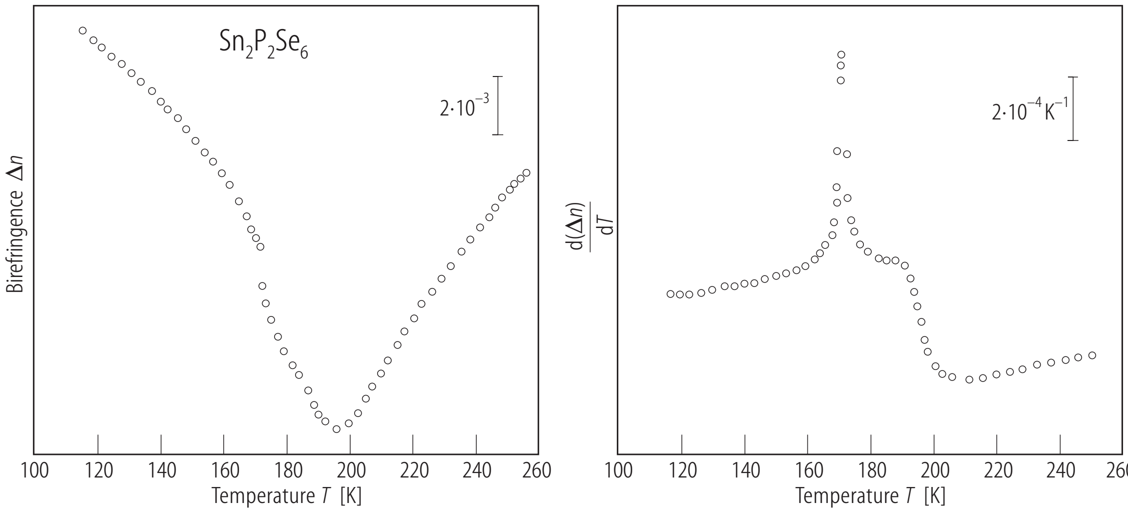

Fig. 24A-2-017. $Sn_2P_2Se_6$. Δn, $\mathrm{d}(\Delta n)/\mathrm{d}T$ vs. T [92Riz]. Incident light propagating along the [100] direction.

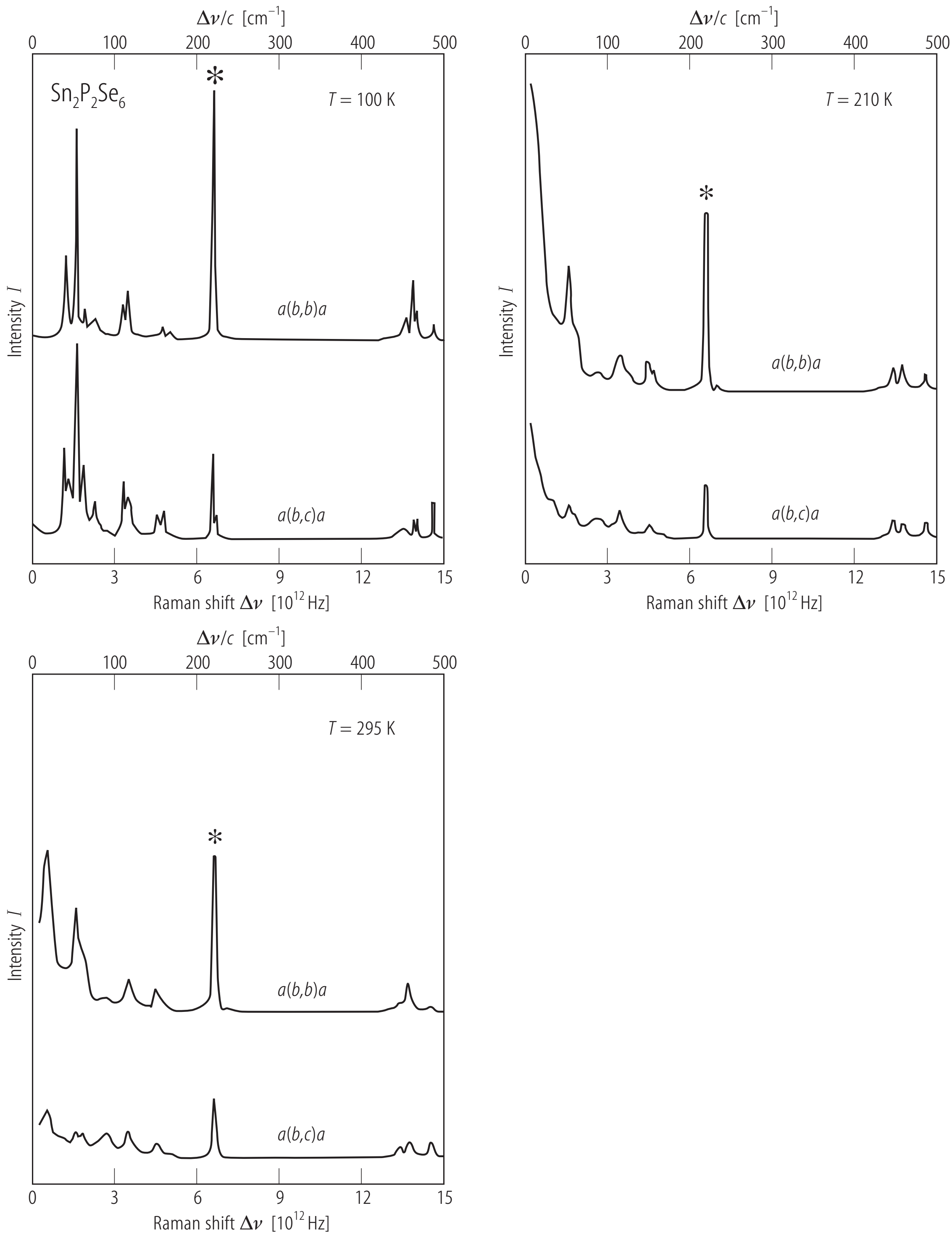

Fig. 24A-2-018. $Sn_2P_2Se_6$. I vs. $\Delta\nu$ [93Loo]. I: Raman intensity, $\Delta\nu$: Raman frequency shift. The intensities of the P–P vibrational modes attached by * in the $a(b, b)a$ spectra are scaled down by a factor 2. Above $12.8 \cdot 10^{12}$ Hz the spectra are scaled up by a factor of 5. $\lambda = 740$ nm.

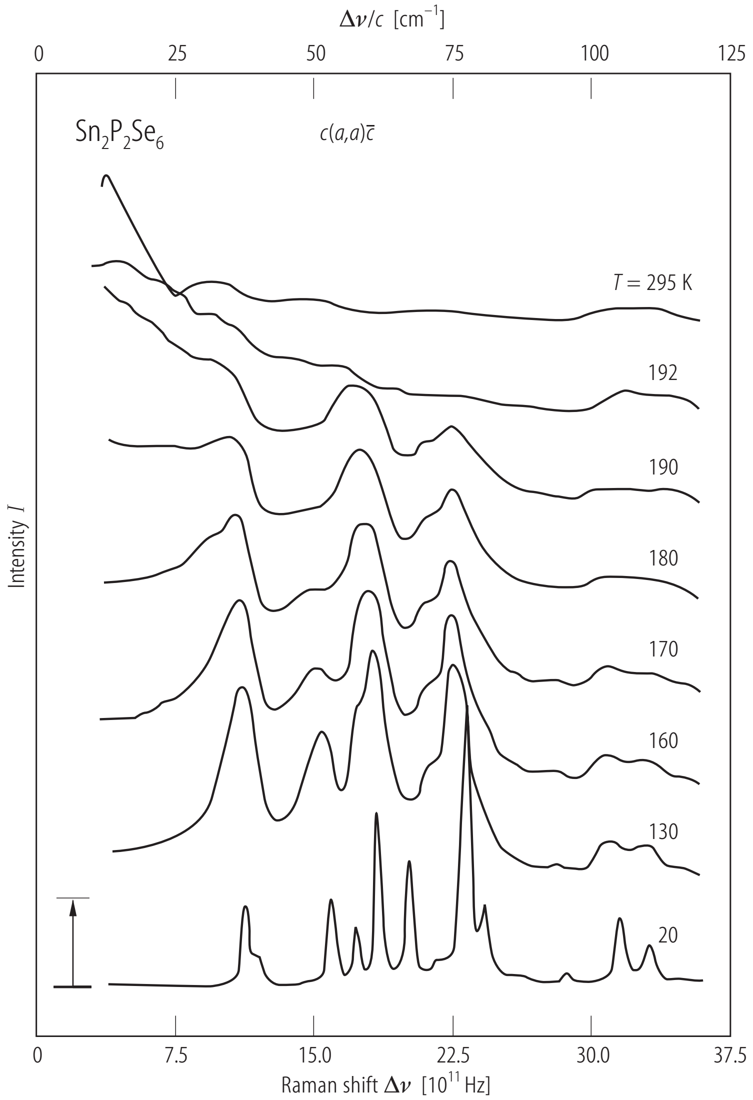

Fig. 24A-2-019. $Sn_2P_2Se_6$. I vs. $\Delta\nu$ [93Loo]. I: Raman intensity, $\Delta\nu$: Raman frequency shift. Parameter: T. Each subsequent curve has been given an offset indicated by the arrow in the lower left corner. $\lambda = 740$ nm.

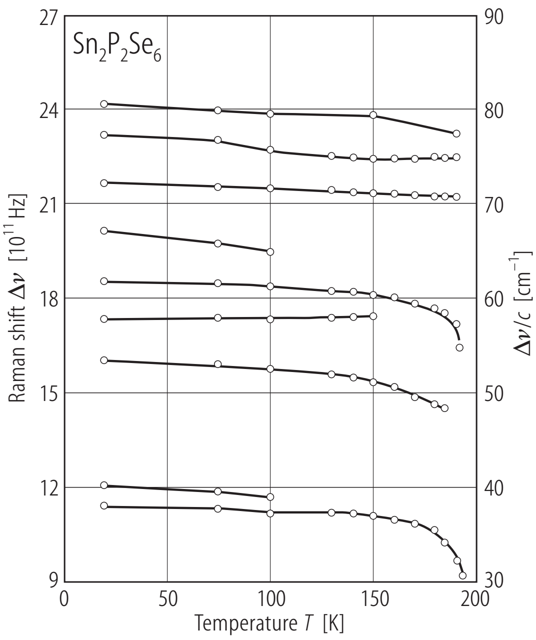

Fig. 24A-2-020. $Sn_2P_2Se_6$. $\Delta\nu$ vs. T [93Loo]. $\Delta\nu$: Raman frequency shift. Parameter: T. $c(a,a)\bar{c}$ scattering geometry. $\lambda = 740$ nm.

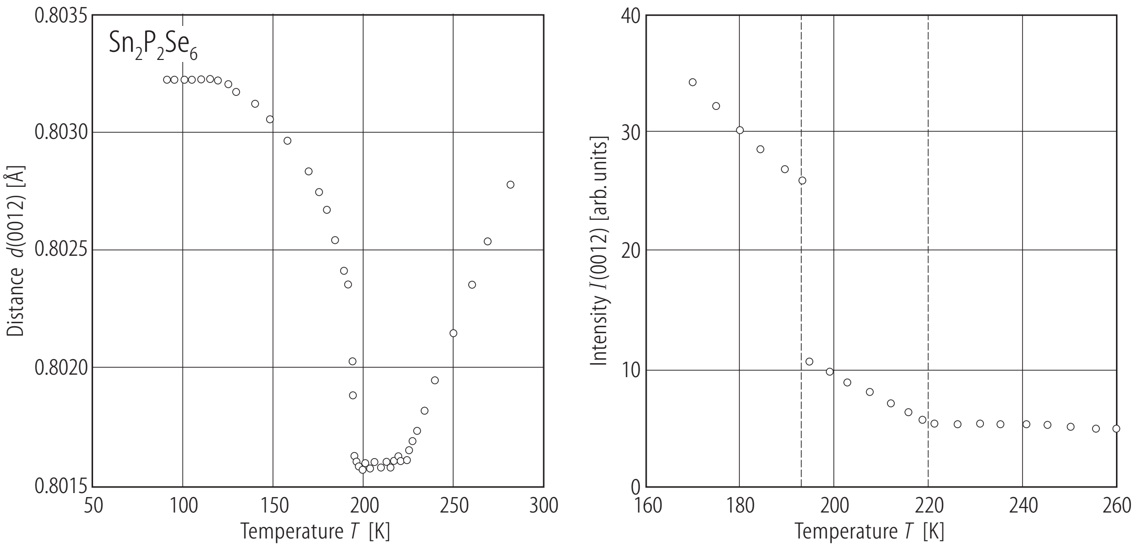

Fig. 24A-2-021. $Sn_2P_2Se_6$. d(0,0,12), I(0,0,12) vs. T [86Bar]. d(0,0,12): interplanar spacing of (0,0,12) planes. I(0,0,12): integrated X-ray intensity of (0,0,12) reflection.

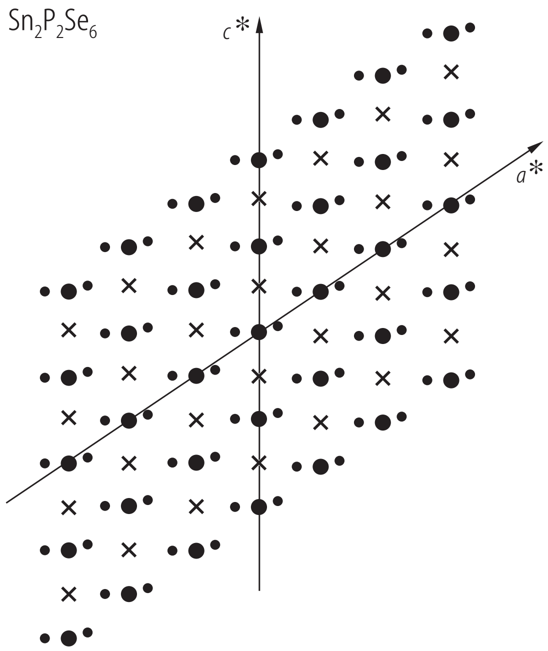

Fig. 24A-2-022. $Sn_2P_2Se_6$. Schematic diffraction pattern of Bragg and satellite reflections in phase II [89Par]. a^*c^*–plane. Full circle: main reflection, dot: satellite reflection, cross: no reflection.

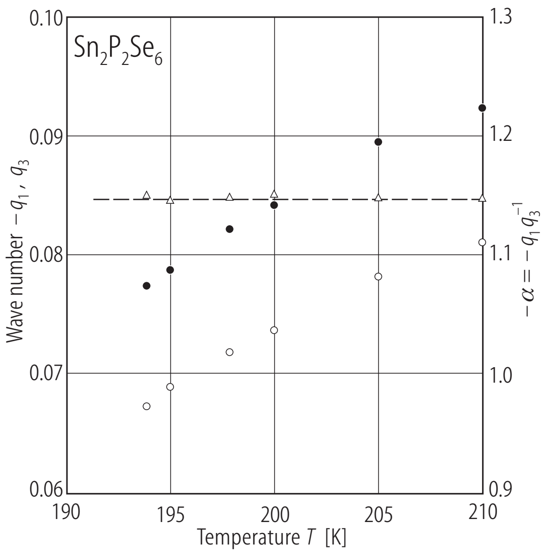

Fig. 24A-2-023. $Sn_2P_2Se_6$. $-q_1$, q_3, $-\alpha$ vs. T [86Bar]. Incommensurate modulation wavenumber is described to $\boldsymbol{q} = q_1\boldsymbol{a}^* + q_3\boldsymbol{c}^*$. α is defined as q_1/q_3, and is equal to –1.146 (4). Full circle: $-q_1$, open circle: q_3, triangle: $-\alpha$.